JOURNAL OF MATERIALS SCIENCE: MATERIALS IN MEDICINE **16** (2005) 393–398

Studies on calcium deficient apatites structure by means of MAS-NMR spectroscopy

L. M. RODRÍGUEZ-LORENZO
ICTP-CSIC, C/Juan de la Cierva 3, 28006-Madrid, Spain
E-mail: luis.rodriguez-lorenzo@ictp.csic.es

The development of synthetic apatites that replicate the features and properties of the contained in natural tissues will help to diminish the misfit between artificial implants and natural hostesses but the structure of these compounds is still under discussion. The variability in Ca/P ratio of calcium deficient apatites has been explained through different models: surface adsorption, lattice substitution and intercrystalline mixtures of hydroxyapatite and octacalcium phosphate. This work investigates which of the models mentioned suits better in a range of samples. Hydroxyapatites obtained by precipitation, by hydrolysis of dicalcium phosphate and calcined samples with Ca/P ratio between 1.50 and 1.77 and specific surface area between 7 and 108 m^2/g have been analysed. OCP and surface adsorption models suit better for great SSA particles and low Ca/P ratio while for smaller SSA particles the lattice substitution model is more accurate. SSA also plays the main role when the capacity to absorb substances is studied though their chemistry can not be explained solely in terms of surface reactivity.

1. Introduction

Biologically formed mineral apatites are characterized as chemically enriched nanosized particles with a low crystallinity. The development of synthetic apatites that replicate the features and properties of the contained in natural tissues will help to diminish the misfit between artificial implants and natural hostesses. The challenge in this task is associated with the structure of these compounds, the compositional variability in apatites [1], which depends upon the synthesis method and possible inhomogeneities attributed to adsorbed substances such as water, carbonates or other ions used during the reaction synthesis.

Although, stoichiometric calcium hydroxyapatite (**OHAp**) crystallizes in the monoclinic $P2_1/b$ spatial group [2], minor quantities of impurities or crystal imperfections leads to the hexagonal $P6_3/m$ in which natural and synthetic apatite compounds have been found to crystallize [3–5]. The complete description of the structure can be found somewhere else [6] but briefly, is made of columns of Ca^{2+} ions spaced by one half of the c-axis parameter along the three-fold axes at 2/3, 1/3, 0 and 1/3, 2/3, 0 which account for two-fifth of the ca^{2+} ions in the structure. Each of these Ca^{2+} ions, Ca(1), is connected to the neighbouring Ca^{2+} ion above and below by three shared oxygen atoms, O(1) and O(2), that lie in the mirror plane of the structure and they are also connected to three further oxygen atoms, O(3), at approximately the same z parameter as the Ca^{2+} ion. These columns of calcium ions and their coordinating oxygen atoms are linked together by phosphate tetrahedra in which three oxygen atoms (two O(3) and either an O(1) or O(2)) come from one column and the fourth (O(2) or O(1) respectively) comes from the adjacent column. The result is a three dimensional network of phosphate tetrahedra with enmeshed columnar calcium ions and with channels passing through it. The axis of these channels coincide with the six-fold screw axes and the corners of the units cells. The remaining calcium ions (Ca(2)) and hydroxyl groups are located in the channels.

The variability in Ca/P ratio of calcium deficient apatites has been explained through different models [4].

1. Surface adsorption [7, 8]. More popular in the past that nowadays is based in the fact that surface phosphates can be protonated or replaced without any restriction imposed by the stoichiometry of the lattice.

2. Lattice substitutions. There are several models for the interpretation of the structure [9] though the most commonly accepted is based on the formulae: $Ca_{10-x}(HPO_4)_x(PO_4)_{6-x}(OH)_{2-x}$. These models are experimentally supported by the analysis of pyrophosphate formed on heating, changes in lattice parameters, infrared (**IR**) and proton nuclear magnetic resonance (^{1}**H NMR**) studies.

3. Intercrystalline mixtures of octacalcium phosphate (**OCP**) and OHAp [10]. This theory is based in the strong structural relationship between OCP and OHAp and it is been supported by single crystal X-ray diffraction (**XRD**) studies, though some studies based on the

IR spectrum and ^{31}P NMR did not found evidence of these intercrystalline mixtures [11].

Solid state nuclear magnetic resonance spectroscopy [12–15] has been used for the analysis of apatite structures. Magic Angle Spinning (**MAS-NMR**) spectroscopy is suitable to investigate both amorphous and crystalline calcium phosphates and can distinguish protonated phosphate groups from unprotonated phosphates groups that are invisible to conventional high resolution NMR spectroscopy [16]. ^{1}H MAS-NMR at 500,13 MHz with a spinning speed of 7.3 kHz has also been shown capable to distinguish between the proton of adsorbed water from the proton from acid phosphate groups and from the proton of the hydroxyl group [12].

This work investigates which of the models mentioned suits better in a range of samples with different stochiometry and particle features that go from stoichiometric hydroxyapatite to calcium deficient apatite and carbonate apatite and from specific surface area (**SSA**) lower than 10 to greater than 100 m^2/g.

2. Experimental

Different methods have been used for the preparation of the apatites. Three of the samples, named ***A***, ***B*** and ***C***, have been obtained by a double decomposition method, described in detail somewhere else [17], by dropping simultaneously $Ca(NO_3)_2{\cdot}4H_2O$, 1 M and $(NH_4)_2(HPO_4)$ 0.66 M at a flow rate of 22 mL/min into a reaction vessel. Rest of conditions as follow; reaction temperature 37 °C for ***A*** and ***B*** and 25 °C for ***C***; reaction time 1 h for ***A*** and ***C*** and 24 h for ***B***; pH 10; maintained with NH_4OH; atmosphere air for ***A*** and ***B*** and CO_2 for ***C***. Sample ***D*** has been synthesized as sample ***B*** plus a calcination step at 800 for 2 h. Sample ***E*** has been prepared following the procedure described in refs [18, 19] by the hydrolysis of dicalcium phosphate at 90 °C for 72 h. Sample ***F*** was prepared following the procedure described in the literature for OCP [20] by dropping a $Ca(C_2H_3O_2)_2$ solution on a K_2HPO_4 solution at 80 °C and pH 4.

Powders were characterized with atomic absorption spectroscopy, Ca was determined using acetylene flame and LaO_2 for background correction. UV-VIS spectroscopy, Phosphorous was analysed using the molibdeno-vanadate method. Both measurements were done in the same solution and Ca/P ratio was calculated from them. The carbonate content was determined by C, H, N analysis in a Perkin Elmer 2400 CHN analyser. Thermogravimetric analyses were performed in a Seiko TG/DTA 320 thermobalance. Fourier transformed infrared spectra (FTIR) were recorded in a Nicolet Magna-IR spectrometer from 500 to 4000 cm^{-1} using the KBr technique and operating in the transmittance mode. X-ray diffraction patterns were recorded with a Phillips X'Pert diffractometer using Cu K_α radiation at 50 mA, 40 kV. Scans were performed in step mode between 2θ values of 4° and 90° and a step size of 0.2° and 10 seconds per step. Morphology of particles was studied by SEM in a Jeol 6400. Specific surface area (SSA) was calculated with the BET method based on the total hysteresis curve obtained in a Micromeritics operating between 10 and 127 Kpa. ^{31}P and ^{1}H MAS-NMR spectra were recorded at a spinning of 13–14.5 kHz and 13.5–14.5 kHz respectively with a Bruker MSL 400P spectrometer. All chemical shift are plotted in ppm from aqueous 85% H_3PO_4 and TMS respectively. Hydration experiments were performed placing the powders in a wet atmosphere at 37 °C for 24 h. MAS-NMR spectra were then recorded again.

3. Results and discussion

FTIR spectra of samples ***A***, ***B***, ***D*** and ***E*** are characteristic of apatite compounds. They show a very strong band between 1000 and 1100 cm^{-1} that can be assigned to the asymmetric stretching band υ_3 of a phosphate group in an apatite environment, a band at 960 cm^{-1} that corresponds to the symmetric stretching band υ_1 and bands at 605 and 575 cm^{-1} that can be assigned to the bending mode. The bands at 3570 and 630 cm^{-1} can be assigned to the vibrational and librational modes of OH^- respectively [21].

FTIR spectrum of ***F*** shows very strong bands at 1024, 1037 and 1057 cm^{-1} that can be attributed to the PO_4 stretching band υ_3 of an OCP and a medium band at 601 cm^{-1} that can be the υ_4 PO_4 bend mode. Strong bands at 1077, 1107 and 1125 cm^{-1} and a medium band at 561 cm^{-1} that can be assigned to υ_3 and υ_4 of a HPO_4 group [22]. Fig. 1 depicts selected spectra of significant samples. ***C*** spectrum also shows bands

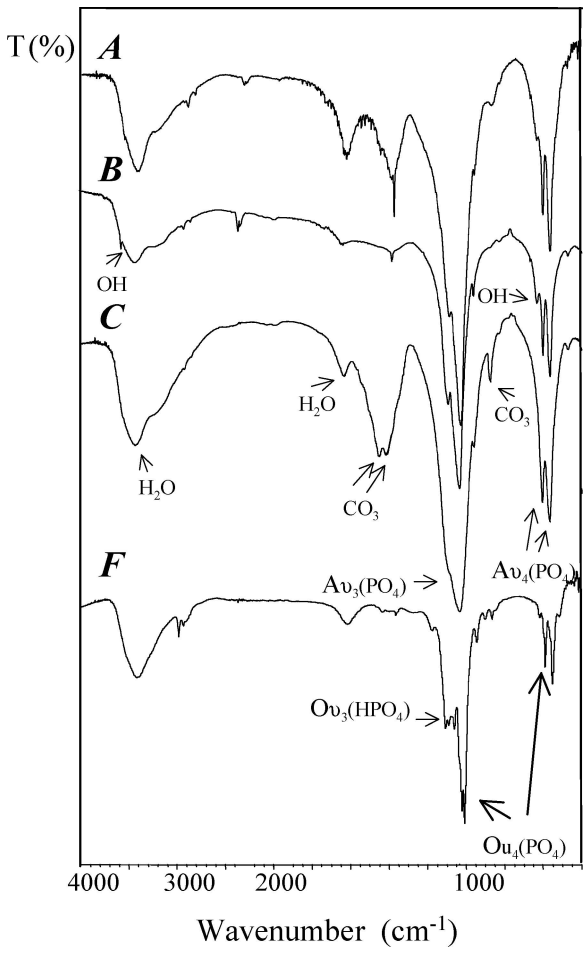

Figure 1 FTIR spectra for samples *A*, *B*, *C* and *F* showing apatite bands (A), and OCP bands (O).

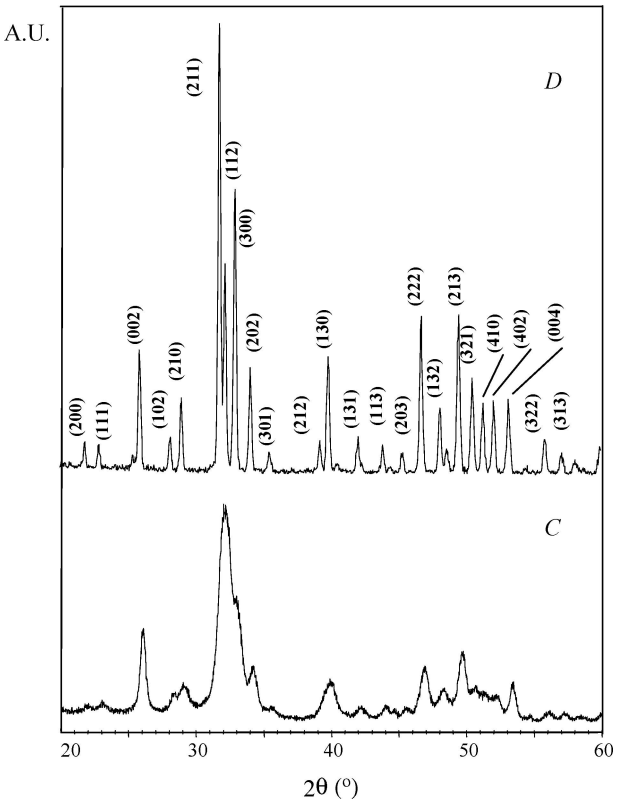

Figure 2 Poorly crystalline (***C***) and well crystallized apatite (***D***) XRD patterns.

at 1416 and 1452 plus a band at 873 cm^{-1} that can be attributed to υ_3 and υ_2 CO_3 modes in a B position in an apatite environment [23]. ***A*** also shows a band at 874 cm^{-1} that can be attributed to a P-O(H) υ_5 mode of the HPO_4^2 [9] plus a band at 1490 cm^{-1} that is attributed to remaining impurities.

XRD patterns of samples ***A***, ***B***, and ***C*** are characteristic of poorly crystalline apatites. *C′* XRD pattern is displayed in Fig. 2 as an example. No peaks that can be assigned to extraneous crystalline phases were found. ***D′*** XRD pattern, also shown in Fig. 2, corresponds to a well crystallised hexagonal apatite phase according to the ICSD file # 26204. No other crystalline phases were identified. ***E′*** XRD pattern corresponds to a single phase crystalline hydroxyapatite. ***F′*** XRD pattern, displayed in Fig. 3 is a triclinic octacalcium phosphate according to ICSD file # 27050.

Calculated cell parameters of the samples identified as apatites are displayed in Table I, together with the Ca/P ratio obtained by chemical analysis. The value of

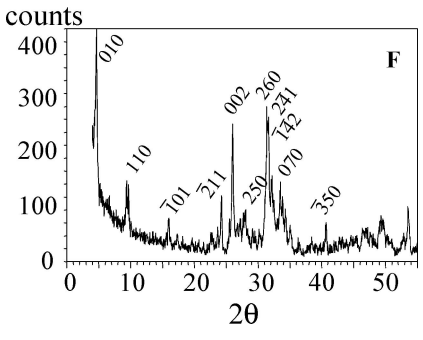

Figure 3 Octacalcium phosphate XRD pattern, sample ***F***.

TABLE I Cell parameters, Ca/ P ratio and SSA of the apatite samples

	Cell parameters			
Sample code	*a*	*c*	Ca/P	SSA (m^2/g)
A	9.453(4)	6.883(4)	1.50	93
B	9.429(6)	6.880(4)	1.67	42
C	9.409(7)	6.895(5)	1.77	108
D	9.4160(2)	6.8801(2)	1.67	15
E	9.4495(2)	6.8877(2)	1.56	7

the *a* cell parameter for ***A***, ***B*** and ***E*** is greater than the value found in the literature for OHAp [3, 8, 24] This could be the result of the presence of HPO_4^{2-} groups substituting for PO_4^{3-} in the structure. It is generally assumed that *a*-axis parameter became slightly larger as the Ca/P ratio decrease [4], but other factors like coprecipitated water can also influence axial parameters [25]. ***A*** and ***E*** are calcium deficient apatites and their IR spectra agree with both explanations, the presence of water and the presence of HPO_4^{2-}, but CO_3^{2-} had to be considered as well. The presence of CO_3^{2-} in the structure of OHAp would lead to lower values of the *a* cell parameter [26]. This is been observed for ***C*** which Ca/P ratio is greater than that of stoichiometric hydroxyapatite. The band at 875 cm^{-1} in the ***C*** IR spectrum was interpreted due to the presence of carbonate groups while for ***A*** and ***E*** had to be due to the acid phosphate group as stated above. ***B*** spectrum does not show a band that can be assigned to HPO_4^{2-} so ***B*** enlarged *a* cell parameter has to be attributed to coprecipitated water.

SSA values are shown in Table I. If it assumed that that there are two surface phosphate ions per surface unit cell and that the (100) form provides all the surface faces, the fraction of surface phosphate ions is SSA/1200. These ions can be protonated or replaced without the restrictions imposed by the stoichiometry of the lattice. This means that for sample ***A*** up to a 7.75% of the phosphates can be replaced. IR spectrum seems to indicate the presence of HPO_4^{2-} groups. A Ca/P ratio of 1.5 implies the replacement of aprox. 17% of the PO_4 groups when the model $Ca_{10-x}(HPO_4)_x(PO_4)_{6-x}(OH)_{2-x}$ is assumed for the calcium deficient apatites [9]. Thus, not all the HPO_4^{2-} groups observed can be attributed to the surface replacement and this fact can explain the enlargement of the *a* cell parameter calculated, though the influence of absorbed water can not be neglected. ***B*** surface phosphate groups are 3.5% of the total phosphates and no acid phosphate groups were found with the IR spectrum neither significant changes in the cell parameters were obtained. ***C*** surface replacement can be up to a 9%. The IR spectrum indicates that the carbonate groups are located on the phosphate position not on the surface and that also could explain the short lattice parameters as commented above. The capacity for surface replacement for sample ***D*** is not greater than 1%, neither acid phosphate groups were observed in the IR spectrum and ***E*** represents a totally different scenario. The percentage of surface phosphates is non greater than 0.6 but HPO_4^{2-} bands were actually found in the IR spectrum and a enlargement on the *a* cell parameter was

TABLE II ^{1}H and ^{31}P MAS-NMR chemical shift, assignments and area under the peak before (bh) and after the hydration experiments (ah)

	^{1}H					^{31}P	
	bh			ah			
	Chemical shift (ppm)	% Area	Assignment	Chemical shift (ppm)	% Area	Chemical shift (ppm)	% area
A	6.62	87.4	Adsorbed water	5.50	93.0		
	0.54	0.4	OCP defect			2.7	
	−0.04	12.0	OH	−0.3	7.0		
B	5.197	56.0	Adsorbed water	5.11	63.4	2.7	
	−0.07	44.0	OH	−0.09	36.6		
C	6.73	97.1	Adsorbed water	6.7	47.0	3.0	
				4.9	51.0		
	0.02	2.9	OH	−0.02	1.5		
D	4.76	22.5	Adsorbed water	4.9	26.0		
	0.03	77.5	OH	−0.6	74.0	2.6	
E	9.75	7.9	Acid phosphate	9.14	8.0		
	6.01	47.5	Adsorbed water	5.69	49.0	2.82	93.6
	0.01	44.6	OH	−0.087	43.0	0.52	6.4
F	10.24	30.1	Acidic proton	10.49	8.9		
	5.08	46.8	Structural H_2O	5.16	54.2		
	2.01	0.6	Mobiledefect	1.97	29.2	2.9	73.4
	1.89	11.3	Mobile defect	1.82	3.5	1.0	26.6
	−0.03	11.2	Disordered OH	−0.09	4.2		

calculated from the XRD pattern suggesting the inclusion of acid phosphate groups within the apatite structure for this sample.

^{1}H MAS-NMR results are shown in Table II. The spectra of ***A*** and ***E*** are displayed in Figs. 4 and 5 as an example of the recorded spectra. The spectrum of sample ***F*** is shown in Fig. 6 including the spectral deconvolution for the different proton species.

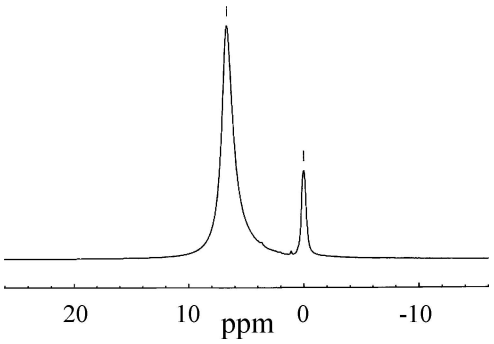

Figure 4 ^{1}H MAS-NMR spectrum obtained from sample ***A*** showing peaks at 6.62, 0.54 and −0.04 ppm attributed to adsorbed water, OCP type defect and OH respectively.

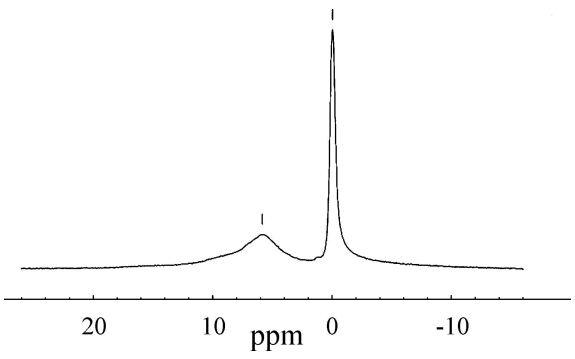

Figure 5 ^{1}H MAS-NMR spectrum obtained from sample ***E*** showing peaks at 9.75, 6.01 and 0.01 ppm attributed to acidic proton, adsorbed water and OH respectively.

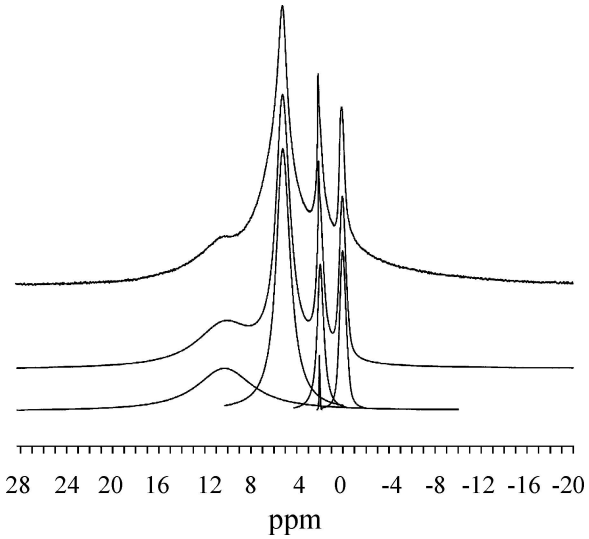

Figure 6 ^{1}H MAS-NMR spectrum and deconvoluted spectra obtained from sample F showing peaks at 10.24, 5.08, 2.01, 1.89, −0.03 ppm attributed to acidic proton, structural water, mobile defects (2.01 and 1.89), and disordered OH respectively.

Spectra of each of the apatites samples (***A–E***) have a peak that can be assigned to the hydroxyl group plus a peak that can be attributed to surface absorbed water. Sample ***A*** also has a peak that could be attributed to an OCP type defect while sample ***E*** has a peak that can be attributed to an acidic proton [12].

The ratios of the area under the peaks attributed to absorbed water and hydroxyl groups are shown in Table III. An exponential increase in the H_2O/OH ratio can be observed for greater SSA as displayed in Fig. 7 while no trend could be appreciated when the Ca/P ratio is considered. This finding seems to indicate the relevance of the particle size, reflected in the SSA, in the reactivity of the products. The smaller Ca/P ratio produces a lower effect even considering the greater

TABLE III Ca/P ratio, carbonate content, SSA and H_2O/OH peak area ratio before (bh) and after (ah) the hydration experiments

Sample	Ca/P	[CO_3] (%)	SSA (m^2/g)	H_2O/OH bh	H_2O/OH ah
A	1.50	1	93	7.26	14.16
B	1.67	<1	42	1.27	1.73
C	1.77	4.8	108	33.4	65.3
D	1.67	<1	15	0.29	0.35
E	1.56	–	7	0.18	1.14

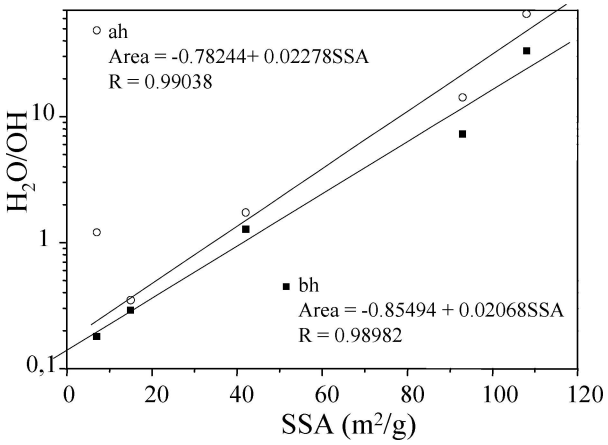

Figure 7 Relationship between area under the peaks and SSA.

number of vacancies and therefore the greater capacity to introduce foreign substances along the hexad channel [27]. The appearance of an OCP-type defect peak for sample ***A*** and an acidic proton peak for sample ***E*** indicates that the OCP theory can suit better for low particle sizes and low Ca/P ratio while the substitution theory suits better for high particle sizes.

^{31}P spectra of ***A–D*** show one single phosphate environment while ***E*** spectrum shows a second environment that can be attributed to the acid phosphate group. The area under this second peak is 6.4% of the total area under the phosphates peaks. These spectra reinforce the idea that for low particle size materials the surface adsorption prevails over the chemical substitution while for greater particle sizes, the effect of the substitution dominates. The spectrum of ***A*** is shown in Fig. 8 as an example of a single environment while ***E*** is displayed in Fig. 9.

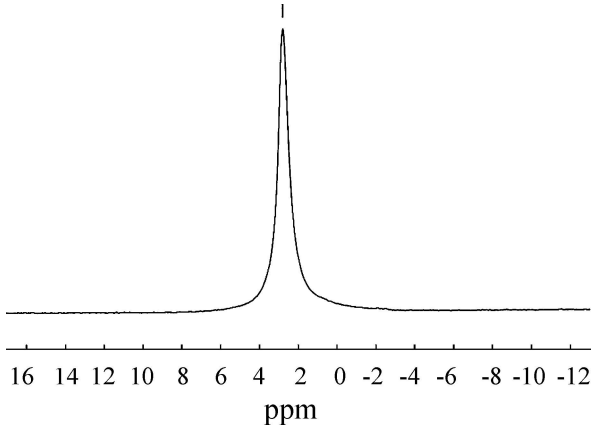

Figure 8 ^{31}P MAS-NMR spectrum from sample ***A*** showing a single phosphate environment at 2.7 ppm.

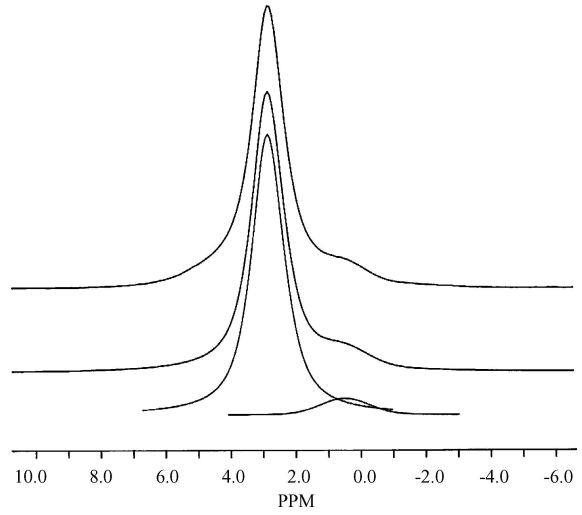

Figure 9 ^{31}P MAS-NMR spectrum from sample ***E*** showing two different phosphate environments at 2.82 and 0.52 ppm.

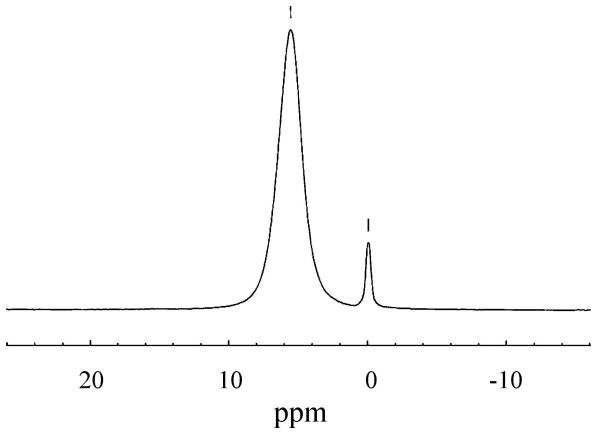

Figure 10 ^{1}H MAS-NMR spectrum from sample ***A*** after hydration experiment showing two peaks at 5.50 and −0.3 attributed to absorbed water and OH respectively.

Hydration experiments were performed in order to check the ability of the apatites to absorb extraneous substances as it is frequently claimed that apatites do [28, 29] and to check whether is related to the structure or the particle features. The spectra of samples ***A*** and ***E*** recorded after the hydration experiments are shown in Figs. 10 and 11 and chemical shifts are displayed in Table II. The spectrum of sample ***A*** does not show the peak attributed to an octacalcium type defect. Only a change in the relative intensity can be observed for ***B***, ***D*** and ***E*** but for ***C*** a new peak can be observed at a chemical shift of 4.9 ppm. The disappearance of the OCP-defect in ***A*** can be related with the hydrolysis of OCP to yield the more stable hydroxyapatite [30]. Peaks at chemical shift between 4.7 and 6.5 ppm have been attributed to absorbed water though the different shifts that suggest different locations. The adsorption of water is still exponential with the increase in surface area as can be observed in Fig. 7 when sample ***E*** is not considered. This result reinforced the prevalence of the SSA as the main factor that influences the reactivity of the apatites for low particle sizes. In sample ***E*** the absorption must be explained in a different way.

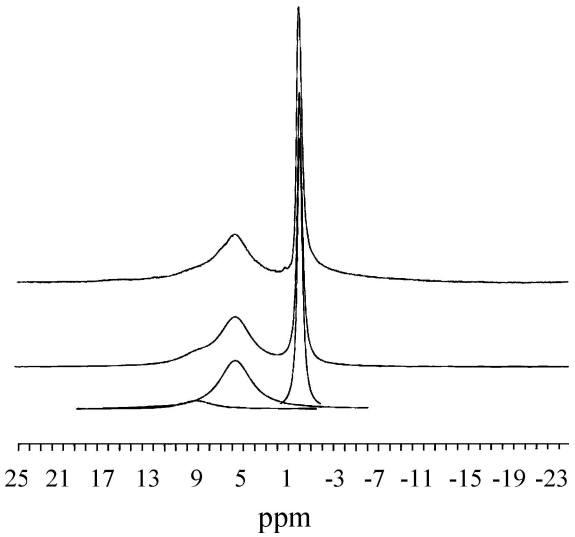

Figure 11 ^{1}H MAS-NMR spectrum from sample ***E*** after hydration experiment showing peaks at 10.49, 5.16, 1.97, 1.82 and −0.09 attributed to acidic proton, structural water, mobile defects (1.97 and 1.82), and disordered OH respectively.

One possibility is the incorporation of water into the hexad channel [27, 31]. Considering two hydroxyl ions along the 6_3 axis of the hydroxyapatite structure, and an ionic ratio of 1.68 Å (6), the total space occupied is $1.68 \times 2 = 3.36$ Å. A c lattice parameter of 6.88 Å allows a space of 6.88–3.36 = 3.52 Å for the introduction of other substances, which is enough to accommodate at least two water molecules. Furthermore, the vacancies created by the calcium deficiency provide extra space that can explain the obtained increase in area under the peak for a sample that has a greater change than the expected when the surface parameters are considered by themselves.

4. Conclusions

The SSA seems to be the key parameter to decide which of the models explain better the structure of calcium deficient apatites. OCP and surface adsorption models suit better for great SSA particles and low Ca/P ratio while for smaller SSA particles the lattice substitution model is more accurate.

SSA also plays the main role when the capacity to absorb substances is considered though calcium deficient apatites can also accept foreign substances along the hexad channel.

Acknowledgments

J. Rocha is acknowledged for performing the hydration experiments and recording the MAS-NMR spectra. The author has been supported by CAM regional government (Spain) through the program to incorporate doctors to the Madrid research system.

References

1. K. A. GROSS, J. N. HART and L. M. RODRIGUEZ-LORENZO, *Key Eng Mater* **218–220** (2002) 165.
2. J. C. ELLIOTT, *Nature* **230** (1971) 72.
3. M. I. KAY, R. A. YOUNG and A. S. POSNER, *Nature* **204** (1964) 1050.
4. J. C. ELLIOTT, "Structure and Chemistry of the Apatites and Other Calcium Orthophosphates" (Amsterdam Elsevier, 1994) Vol. 18.
5. L. M. RODRIGUEZ-LORENZO, J. N. HART and K. A. GROSS, *J. Phys. Chem. B* **107** (2003) 8316.
6. M. I. KAY, R. A. YOUNG and A. S. POSNER, *Nature* **204** (1964) 1050.
7. W. E. BROWN, *Clin. Orthop. Rel. Res.* **44** (1966) 205.
8. J. C. J. ARENDS, M. R. CHRISTOFFERSEN, H. ECKERT, B. O. FOWLER, J. C. HEUGHEABAERT, G. H. NANCOLLAS, J. P. YESINOWSKI and S. J. ZAWACKI, *J. Cryst. Growth* **84** (1987) 515.
9. E. E. BERRY, *J. Inorg. Nucl. Chem.* **29** (1967) 317.
10. W. E. BROWN, J. P. SMITH, J. R. LEHR and A. W. FRAZIER, *Nature* **196** (1962) 1050.
11. W. P. ROTHWELL, J. S. WAUGH and J. P. YESINOWSKI, *J. Am. Chem. Soc.* **102** (1980) 2637.
12. J. P. YESINOWSKI and H. ECKERT, *ibid.* **109** (1987) 6274.
13. K. BESHAH, C. REY, M. J. GLIMCHER, M. SCHIMIZU and R. G. GRIFFIN, *J. Solid. State Chem.* **84** (1990) 71.
14. Y. WU, J. L. ACKERMAN, H. KIM, C. REY and A. G. BARROUG, *J. Bone Miner. Res.* **17** (2002) 472.
15. T. ISOBE, S. NAKAMURA, R. NEMOTO, M. SENNA and H. SFIHI, *J. Phys. Chem. B* **106** (2002) 5169.
16. J. P. YESINOWSKI in "Calcium Phosphate in Biological and Industrial Systems," edited by A. Z. (Kluwer Academic Publishers, Boston, 1998).
17. L. M. RODRÍGUEZ-LORENZO and M. VALLET-REGI, *Chem. Mater.* **12** (2000) 2460.
18. A. MORTIER, J. LEMAITRE, L. RODRIQUE and P. G. ROUXHET, *J. Solid. State Chem.* **78** (1989) 215.
19. R. M. WILSON, J. C. ELLIOTT, S. E. P. DOWKER and L. M. RODRIGUEZ-LORENZO, *Biomaterials* **26** (2005) 1317.
20. R. Z. Le GEROS, *Calcif Tissue Int.* **37** (1985) 194.
21. B. O. FOWLER, *Inorg. Chem.* **13** (1974) 194.
22. B. O. FOWLER, M. MARKOVIC and W. E. BROWN, *Chem. Mater.* **5** (1993) 1417.
23. C. REY, B. COLLINS, T. GOEHL, I. R. DICKSON and G. M. J., *Calcif. Tissue Int.* **45** (1989) 157.
24. K. SUDARSSANAN and R. A. YOUNG, *Acta. Cryst. B* **25** (1969) 1534.
25. R. A. YOUNG and D. W. HOLCOMB, *Calcif. Tissue Int.* **36** (1984) 60.
26. R. Z. LeGUEROS, "Calcium Phosphates in Oral Biology and Medicine", (Karger Basel, 1991) Vol. 15.
27. V. MICHEL, P. ILDEFONSE and G. MORIN, *Appl. Geochem.* **10** (1995) 145.
28. R. Z. LEGEROS, "Calcium Phosphates in Oral Biology and Medicine" (Karger Basel, 1991) Vol. 15.
29. L. M. RODRIGUEZ-LORENZO, J. N. HART and K. A. GROSS, *Biomaterials* **24** (2003) 3777.
30. W. E. BROWN, M. MATHEW and M. S. TUNG, *Prog. Cryst. Growth Charact.* **4** (1981) 59.
31. R. M. WILSON, J. C. ELLIOTT, S. E. P. DOWKER and R. I. SMITH, *Biomaterials* **25** (2004) 2205.

Received 1 July
and accepted 1 November 2004